Journal of Energy and Safety Technology

JEST

RESEARCH ARTICLE Open Access

EFFECT OF THE GEOMETRY AND MOORING LINE ON THE HYDRODYNAMICS OF A PONTOON MODEL FOR MARINE FLOATING PHOTOVOLTAICS

D. H. Harahap[1], A. D. Rictanata[2] and H. D. Armono[3]

[1]Magister of Innovation and System Technology, School of Interdisciplinary Management and Technology, Institut Teknologi Sepuluh November, Surabaya, Indonesia.
[2]Physic Engineering, Faculty of Industrial Technology and System Engineering, Institut Teknologi Sepuluh November, Surabaya, Indonesia.
[3]School of Interdisciplinary Management and Technology, Institut Teknologi Sepuluh November, Surabaya, Indonesia.

Corresponding author: danieldevy.2@gmal.com

Article History

Received:	Received in revised form:	Accepted:	Published:
July 15, 2025	December 1, 2025	December 22, 2025	December 26, 2025

Abstract

This study aimed to analyze the effects of different pontoon models, including variations in pontoon geometry and mooring lines, on the hydrodynamic responses of marine floating photovoltaic (FPV) systems using numerical models. The examined variables included the geometric shapes of the pontoons, the number of mooring lines, irregular wave patterns, and water depth. The results demonstrate that adding pontoons with breakwater geometries—specifically cylindrical and rectangular shapes—results in lower hydrodynamic responses than the Pure float model. Among the models tested, the breakwater configuration achieved the most significant reduction in hydrodynamic responses, with a decrease of 59% across the six degrees of freedom (DOF). The rectangular model was closely followed, with a 56% reduction, whereas the cylindrical model showed a 47% reduction. The use of six mooring lines can further minimize the effects of wave excitation and hydrodynamic responses across the six DOFs. On average, adding the mooring lines resulted in a 27% reduction in the response amplitude operator (RAO) values and a 9% decrease in the mooring line tension. This research provides valuable hydrodynamic performance insights for designing a marine FPV system, serving as a practical guide for preliminary design consideration while acknowledging that comprehensive design requires additional cost, manufacturing, and structural assessments.

Keywords: Marine Floating Photovoltaic (Marine FPV), Breakwater Mooring Line, Response Amplitude Operator (RAO).

1.0 INTRODUCTION

The increase in energy needs has become essential in recent years. Various efforts and proactive strategies have been undertaken by multiple parties to reduce carbon emissions from fossil fuels [1] to optimize the utilization of energy in all sectors. To overcome these issues, the use of renewable energy as an alternative energy source was further developed. This commitment was manifested through the G20 Presidency event in Indonesia in 2022 with one of the main topics being the transition to renewable energy [2]. Furthermore, the government is also committed to increasing the renewable energy mix by 23% in 2025 [3], which is covered in the Indonesian National Electricity Supply Business Plan from 2021 to 2023. This strategy is also supported by the government's progressive efforts in increasing the electrification ratio in the least developed, frontier, and outermost (3T) regions, which in 2022 is at 90.78%, with some other provinces still standing at 80% (West Kalimantan, North Kalimantan) and 50% (Papua and West Papua provinces) [4]. One novel technology that has been actively developed is floating photovoltaics (FPV). This system uses solar panels installed on

pontoons and floated on a water body [5]. The purpose of the on-the-water-body installation is to make the best use of the area and to increase the module's efficiency by allowing natural cooling from the water body underneath it. This natural cooling may increase the efficiency of the system up to 11% [7]. The potential development of floating photovoltaic energy sources in Indonesia is massive, primarily due to its geographical condition as the biggest archipelago country in the world with 17.508 islands, 81.000 km of coastline, 521 lakes, and more than 100 reservoirs [6], [8]. A crucial component of an FPV is a floater or the pontoon. This component also ensures that solar panels and other electrical components remain floating and provides access for operation and maintenance purposes [5]. An FPV normally uses a rectangular or cylindrical platform, where the panels and their supporting components will be put atop pontoons [5]. The design of the pontoon may vary depending on the manufacturer. In 2020, at least 2 GW of FPVs were installed around the world[10]. Floating photovoltaics has begun to be developed on some projects that may be installed in marine environments and able to withstand corrosion and maritime environment [11]. Research performed on FPVs generally manifests as behavioral analysis from the system, primarily on FPVs installed on certain water bodies [12]–[14]. Recent advancements in 2024 have further elucidated hydrodynamic behavior of floating structures in marine conditions [33, 34]. Hydrodynamic studies are also crucial to determining a floating system's design, stability, and safety, mainly for operation and maintenance [15]. Due to the vastness of its development potential and marginal research regarding the hydrodynamic response to marine FPVs, research on the influence of pontoon geometry and mooring line variations on the hydrodynamic response of marine FPVs has been conducted.

2.0 METHODOLOGY

2.1 Floating Photovoltaic (FPV) and Mooring Line

Floating photovoltaic panels are one of solar PV's applications whereby the panels are designed and installed atop pontoons on a water body such as a reservoir, weir, pool, or lake. In this system , solar panels are generally installed on a floating structure with a fixed location by mooring it to an anchor and a mooring line [9]. On the mooring line, mathematical approaches are applicable to describe the force and variables working on the usage of a mooring line. These forces result from various physical parameters that influence the movement and tension of a mooring line under specific operating conditions. Equation (2.1) describes the dynamic movements of the mooring line [16]

$$W_i + T_i + D_i + F_i^M + F_i^r + F_i^v + F_i^f = F_i^{tot} \tag{2.1}$$

Remarks:
Wi = *Weight* (N)
Ti = Line tension (N)
Di = Drag force (N)
F_i^M = Marrison force (N)
F_i^r = Seabed Reaction force (N)
F_i^v = Vertical Seabed Reaction force (N)
F_i^f = Seabed friction force (N)

2.2 Modeling Assumptions and Justification

The numerical simulations employed linear wave theory for irregular wave conditions (Hs = 0.38-0.63 m), justified by wave steepness parameter $H/gT^2 < 0.01$. Viscous effects were incorporated through Morison's equation using established drag coefficients for similar offshore structures. Boundary conditions included a fixed seabed with non-linear catenary mooring lines representing Indonesian nearshore conditions. Platform modeling used rigid body dynamics with mass properties from Table 4.1, representing typical FPV construction materials.

2.3 Hydrodynamic Load Model

Three mechanical principles can be applied to an FPV if installed on the sea, i.e. Inertia, gravity, and viscous effects [19]. This equation is shown in (2.2).

$$F^H = \sum \Delta F_n^{FK} + \sum \Delta F_n^S + \sum F_n^R + \sum \Delta F_n^D \tag{2.2}$$

Remarks:
F_n^H = Hidrodinamik force (N)
F_n^{FK} = Froude-Krylov force (N)
F_n^R = *Radiation* force (N)

F_n^S = diffractive force (N)
F_n^D = *Viscous* force (N)

The Morison equation is intended for a moving floating object on a fluid, as shown in (2.3) equation [21]

$$F = \underbrace{\rho V \dot{u}}_{a} + \underbrace{\rho C_a V (\dot{u} - \dot{v})}_{b} + \underbrace{\frac{1}{2}\rho C_d A (u - v)|u - v|}_{c}. \quad (2.3$$

Remarks:
u = *water* flow acceleration (m/s)
h = *wave* height (m)
ω = Angular frequency (rad/s)
k = wavenumber
H = water depth (m)

2.4 Floating Structure in 6 Degrees of Freedom (6 DOF)

On a floating structure with a known distributed mass, its motion can be analyzed using the coupled equation in 6 DOF. [17].

$$(m_j + a_{jj})\,\ddot{x}_{j(t)} + b_{jj}\dot{x}_{j(t)} + c_{jj}x_{j(t)} = f_{j(t)} \quad (2.6)$$

Remarks:
m_j = Mass (kg)
a_{jj} = *Added Mass Coefficient*
b_{jj} = *Damping Coefficient*
c_{jj} = *stiffness*
x = Motion (m)
$\dot{x}$ = Velocity (m/s)
$\ddot{x}$ = Acceleration (m/s^2)

The excitation force can be broken down as follows:

$$f_{j(t)} = f_{jo}\cos(wt) \quad (2.7)$$

2.5 Response Amplitude Operator (RAO)

The RAO value is used to determine the response of a *floating body* when operating on a specific *water body*. The general equation of motion in the frequency domain can be broken down as in (2.8) equation:

$$[M + A(\omega)]\ddot{x} + B(\omega)\dot{x} + Cx = F(\omega) \quad (2.8)$$

Remarks:
x = *rigid body* motion (m)
ω = Oscillation frequency (Hz)
M = Mass and structure inertia (kg)
$A(\omega)$ = *Added Mass Coefficient*
$B(\omega)$ = *Linear Damping Coefficient*
C = *Restoring Force Coefficient*

Meanwhile, the RAO can mathematically be defined as the ratio between the response amplitude and the wave amplitude for a linear system in which is plotted against *wave frequency* or *wave periods* [21].

$$Z_j(\omega, \theta) = \frac{[X_k(\omega)]}{D_j} = [H_{jk}(\omega)]^{-1}[F_j(\omega)], \quad (2.9)$$

Remarks:
Zj (ω, θ) = Amplitude at frequency ω, direction θ
Xk (ω) = Motion (m)
Dj = Wave's amplitude (m)
Fj (ω) = Wave's excitation force (N)

2.6 Literature review, Parameter identification, and problem Formulation

A literature study is conducted to deepen the comprehension of the required information as a support element in research. The conducted literature studies on FPV, Floating Platform, and Response Amplitude Operator related studies. The Hydrodynamic response is used as a determining parameter for system stability , which in turn shall affect the energy production from a Floating Photovoltaic system. This is due to the motion from the system's structure on a water body which will affect the panel's tilting angle of a solar panel, thus affecting energy production of an FPV system [23], [24]. Therefore, an analysis of the hydrodynamic response of a Marine FPV and its influential parameters is very crucial to be conducted.

2.6.1 Environmental Parameter

The simulation parameters were selected based on typical conditions for coastal floating photovoltaic deployments. Water depth variations of 10, 15, and 20 meters represent common ranges for nearshore installations. Wave condition utilized significant wave heights of 0.38 – 0.63 m with peak periods of 4.0 – 5.0 s, representing moderate sea states in sheltered coastal waters. Mooring configurations followed conventional design used in similar floating structure applications.

2.7 Pre-processing

The preprocessing stage involves designing a system for a 30-kWp marine FPV. The design of each pontoon will be the first stage physical properties that can be obtained from each model. This input function describes the model's physical condition, which will be made as the main basis of the simulation. The geometry model is then exported as a step file format. The program preprocessing stage is conducted using two features i.e. Design Modeler and Meshing.

After establishing the Setup Model in the Design Modeler, one must apply meshing to each model. Since the software's computations rely on the interactions between a floating object and water, surface meshing is required. This means that the elements and nodes are generated solely on the model surface. [25]. In the meshing stage, it is necessary to verify and optimize the meshing configuration so that maximum output can be obtained with a minimum computation load. The verification process of meshing was conducted using the Grid Independence Test, by varying the element size meshing and comparing the RAO output results for each variation.

2.8 Processing

The simulation employs Hydrodynamic Diffraction and Hydrodynamic Response to determine the Response Amplitude Operator (RAO) for each variation. The variations included changes in the pontoon geometry shape, number of mooring lines, wind speed, wave conditions, and water depth, totaling 72 different combinations. The irregular wave conditions utilized are:

- Irregular Wave 1: Hs = 0.38 m, Fp = 0.31 Hz
- Irregular Wave 2: Hs = 0.50 m, Fp = 0.28 Hz
- Irregular Wave 3: Hs = 0.63 m, Fp = 0.25 Hz

The water depth variations were based on typical nearshore conditions: 10 meters, 15 meters, and 20 meters. Regarding mooring lines, the simulation considers two variants: 4 mooring lines and 6 mooring lines. The length of each mooring line ranged from 20 to 50 m with angles between 30 degrees and 45 degrees.[25].

The wave direction parameters extend from -180 degrees to 180 degrees, while the automatic wave frequency is determined by the system based on the geometry meshing results. The output from the Hydrodynamic Diffraction analysis includes hydrostatic properties such as the Center of Gravity, Center of Buoyancy, and Metacenter. After modeling with Hydrodynamic Diffraction, the models undergo further simulation with Hydrodynamic Response to obtain the RAO in the frequency domain, which will then be visualized.

Once the RAO has been calculated, the data from the Hydrodynamic Response simulation will be compared to the RAO standards set by PIANC (World Association for Waterborne Transport Infrastructure) [7].

3.0 RESULTS AND DISCUSSION

3.1 Verification

The conducted verification in the research is geometry model verification on Software as an initial condition and GIT, using varying element size meshing and comparing RAO output results on each variation. After the GIT was conducted, the obtained element size result on the Purefloat Model is 175 mm, on the rectangular model is 198 mm, on the cylindrical model is 205 mm, and on the Breakwater, model is 185 mm. The meshing method on those four models uses the triangle

method because this method is the most effective and efficient[26]. The element size selection for each geometry is based on the differential percentage between the resulting outputs with tolerance as big as 10% [27], [28]. At this tolerance percentage, the output value of each simulation doesn't significantly change. The Surge RAO value (X axis) was the compared output against the GIT process. The Surge RAP value at 0.503 Hz is selected to be compared so that the most optimum element size value could be discovered to simulate the model, with minimum computational load and optimum result.

3.2 Validation

During the validation process, the hydrostatic values obtained from the simulations were compared with those derived from the analytical calculations, with an allowable error tolerance of 10% [27]. This method was similarly employed by Ibinabo (2019) to validate the simulation results by comparing the output values with manually calculated values. The hydrostatic variables for comparison include the center of gravity (CoG) on the Z-axis, Volume Displacement, and Water Plane Area. The model selected for this validation is the Rectangular Model.

The detailed properties of the Rectangular Pontoon are as follows: the differences in error for CoG, Volume Displacement, and Water Plane Area were found to be 0%, 0.16%, and 5.91%, respectively. The error percentages obtained from comparing the simulation results with the analytical calculations were all below the 10% threshold, thereby meeting the standard for error values.

3.3 The Effects of Geometry Variations Towards Response Amplitude Operator (RAO)

3.3.1 Physical Mechanisms of Geometry Effect on Hydrodynamic Response

The variation in RAO responses across different pontoon geometries arises from distinct hydrodynamic interactions. Breakwater configurations introduce additional virtual mass that elevates the system's inertia, particularly for rotational movement, thereby lowering resonant frequencies. The expanded surface area of these geometries promotes more effective energy dissipation through wave radiation, while flow separation around structural components generates supplementary damping. Furthermore, the strategic placement of secondary pontoons establishes interference patterns in wave forces, leading to partial cancellation of excitation loads. These combined physical phenomena contribute to the observed enhancement in motion response characteristics for breakwater-type floating structures.

3.3.2 Result and Analysis

In the conducted research, 4 variants of the pontoon geometry models are used for the Marine FPV system. The four geometry models are as follows: Purefloat, Rectangular, Cylindrical, and Breakwater (figure 4.1 – 4.4).

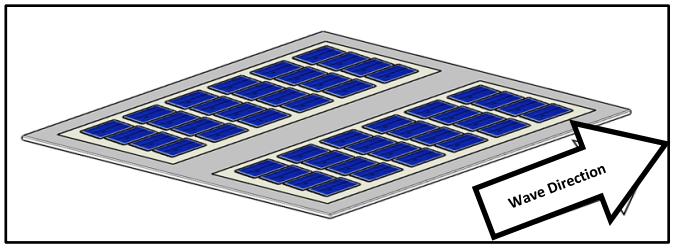

Figure 4. 1 Purefloat Model

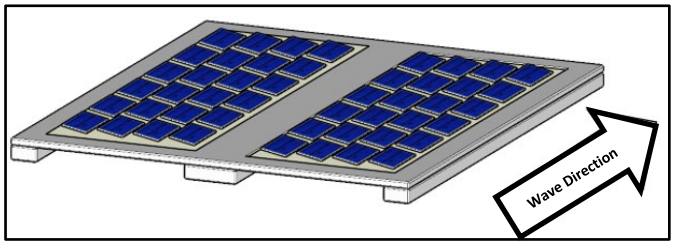

Figure 4. 2 Rectangular Model

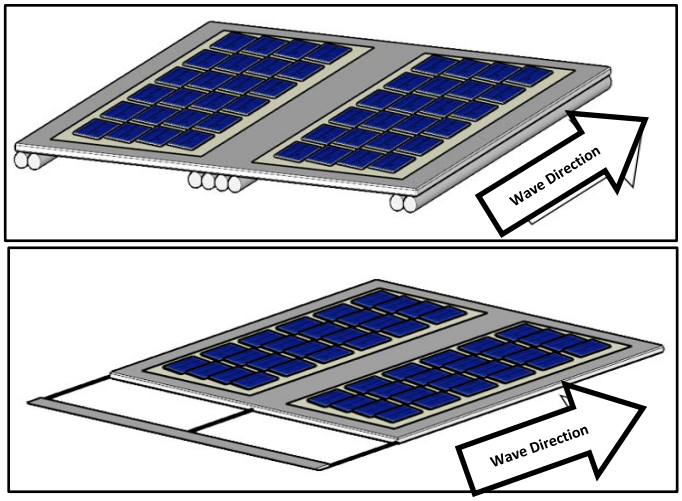

Figure 4. 4 Breakwater Model

Table 4. 1 Properties of the Model Geometry

No	Properties	Model	Model 2	Model3	Model 4
1	Mass (kg)	25959.7	58778.8	52343.7	27424.6
2	Volume (m^3)	27.2	61.7	54.9	28.8
3	Length (m)	17.3	17.3	17.3	17.3
4	Width (m)	15.2	15.2	15.2	15.2
5	Height (m)	0.386	0.886	0.876	0.386
6	Ixx ($kg.m^2$)	578300	1420000	1258000	607700
7	Iyy ($kg.m^2$)	841600	1670000	1515000	1093000
8	Izz ($kg.m^2$)	1419000	3083000	2767000	1700000

The parameters listed in Table 4.1 were used as inputs for the RAO calculation process by the numerical analysis software. This calculation is based on the positional changes of the Center of Gravity floating platform [25]. The RAO analysis is divided into translational and rotational movements. A translational motion is the motion of an object on a straight trajectory without any rotation. In the 6 DOF theory, the motions that belong to translational are Surge (X-axis), Sway (Y-axis), and Heave (Z-axis). Figure 4.5 shows the translational motion's RAO that occurs on a floating pontoon within the 0.20 Hz – 0.70 Hz frequency range. The RAO value in each model values compared to the water conditions at a depth of 10 m and the impulse in the form of irregular wave at 0^o incoming waves.

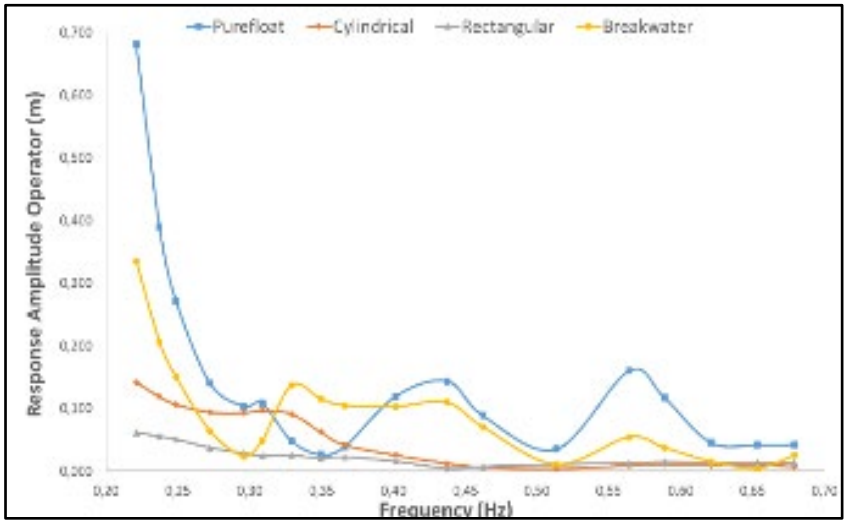

Figure 4. 5 RAO Surge 4 Mooring line

The RAO surge Purefloat value was smaller than the Rectangular, Cylindrical, and Breakwater is due to the wave hitting the pontoon model from the sides (the incoming angle: 0°, or positive X-axis direction), which had smaller areas compared to the front and rear sides.

The Morrison equation is a mathematical model used to calculate the amount of force exerted on a floating structure due to the interaction between the structure and waves. This equation is a summation of the inertial and drag forces on the floating structure as shown in Equation (2.3). One of the key variables influencing the force exerted on a floating structure is the cross-sectional area (A).

The Morrison equation can be further developed into a Hydrodynamic Load Model for a floating structure, as described in Equation (2.2). This model illustrates that in a Floating Solar System, three main forces are at play: Inertia, Gravity, and Viscosity. A crucial parameter in determining the Hydrodynamic Force is the Froude-Krylov (F^{fk}) force, which is directly proportional to the cross-sectional area of the structure. Consequently, a larger area results in a greater wave excitation effect on the floating structure.

The introduction of a secondary pontoon on the bottom side of the main pontoon (in the Purefloat model, based on cylindrical and rectangular shapes), increased the overall thickness, volume, and mass of the structure. The cylindrical and rectangular models exhibit RAO (Response Amplitude Operator) surge values with low peak propensity across both lower and higher frequency ranges. Graphs depicting the RAO for Sway motion (Y-axis translation) and Heave motion (Z-axis translation) for the four geometric models are shown in Figures 4.6 and 4.7. graphic

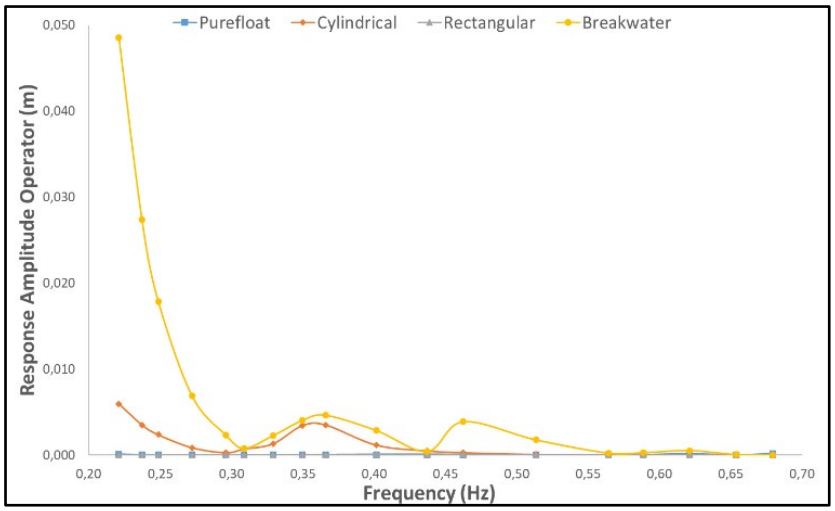

Figure 4. 6 RAO Sway 4 Mooring Line

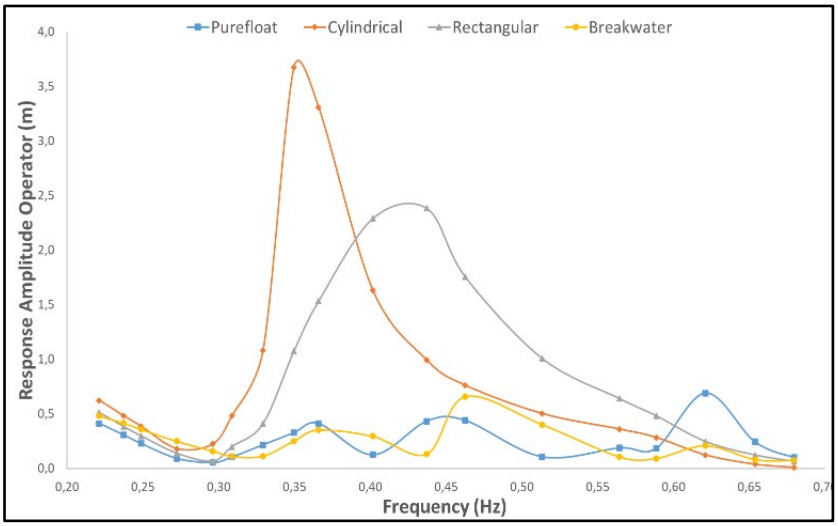

Figure 4. 7 RAO Heave 4 Mooring line

The result from the RAO graphic in sway motion (Y axis) and heave motion demonstrates a similar propensity for four geometric models (Rectangular, cylindrical, and breakwater models) as what happens to RAO surge motion. Nilai. The highest heave values occurred at 4 m in the cylindrical model, 2 m in the rectangular model, 0.6 in the Purefloat model,

and 0.6 m in the Breakwater model. On the other hand, for rotational motion RAO (Roll, pitch, and yaw) at a depth of 10 m, the frequency range is 0.20–0.70 Hz, irregular wave type 1, with 4 mooring lines as shown on Figure 4.8 to 4.10.

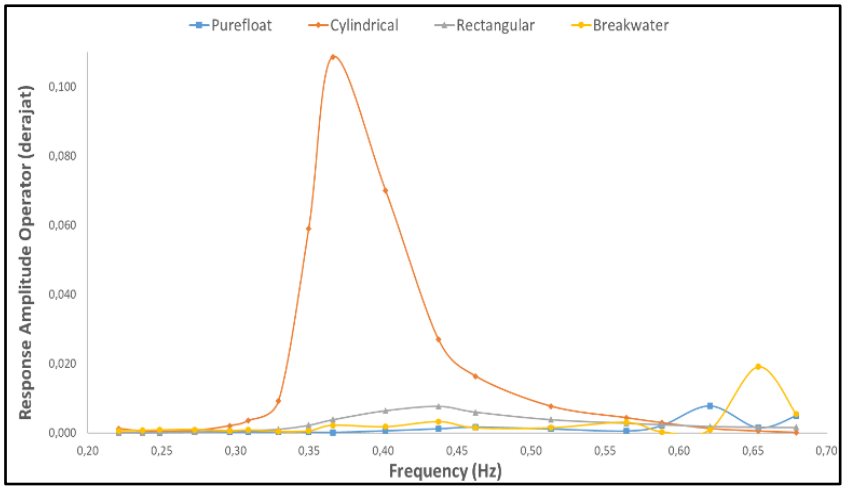

Figure 4. 8 RAO Roll 4 Mooring Line

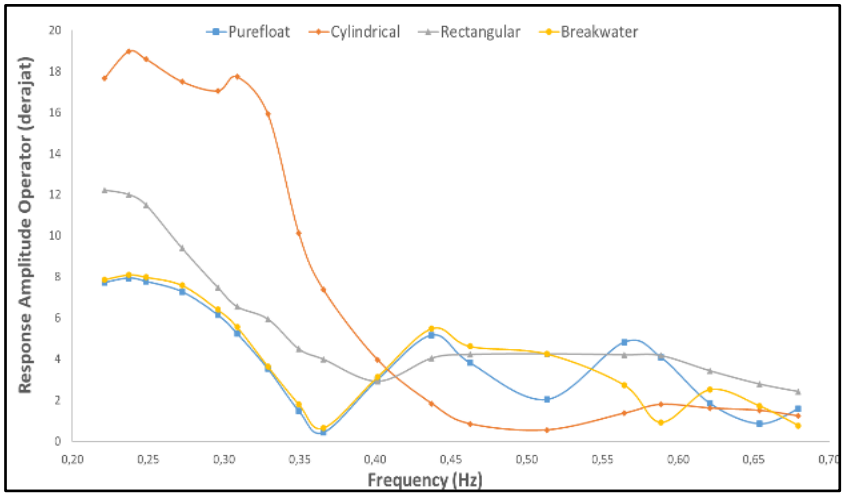

Figure 4. 9 RAO Pitch 4 Mooring Line

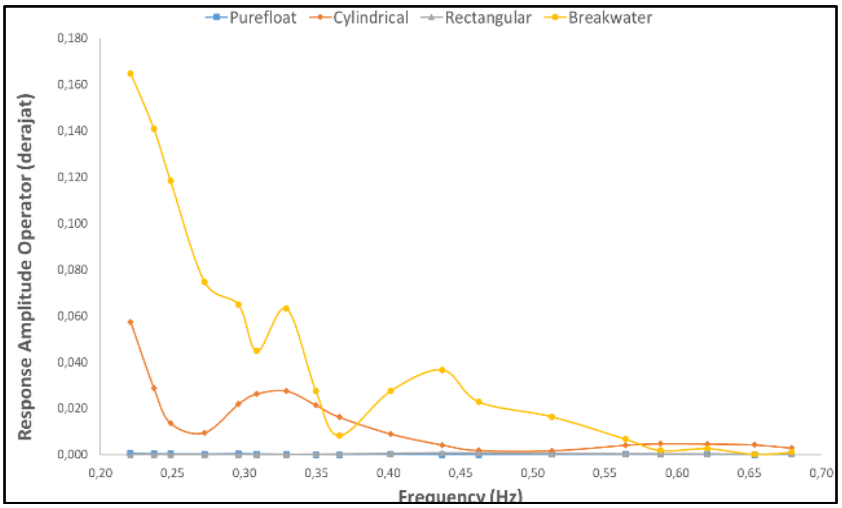

Figure 4. 10 RAO Yaw 4 Mooring Line

The results of the marine FPV system simulation, focusing on variations in the Poonton geometry, reveal significant differences in the Response Amplitude Operator (RAO) values for both translational and rotational motions. For specific motions such as surges, sways, rolls, and yaw, the RAO values for the Breakwater and Purefloat models exhibit very high peaks at low frequencies. Although these RAO values generally decrease with frequency, the differences between the rectangular and cylindrical models remain substantial.

The RAO value measures the amplitude of a floating system in terms of the excitation force exerted by waves. A lower RAO value indicates better performance for a floating structure, and vice versa. According to the simulation results, the breakwater model demonstrates a smaller RAO value than the purefloat, and cylindrical models.

To quantify the extent of changes in the RAO for each model, a statistical approach known as analysis of variance (ANOVA) was employed. Moreover,tThis method compares the differences between groups [29] and within groups, allowing for a clear understanding in the magnitude of changes. The changes can be quantified by calculating the mean (average) percentage change in RAO values between models and comparing them against the baseline model, which is the Purefloat model. Table 4.2 illustrates the percentage reduction of RAO for each geometry model relative to the Purefloat model for six degrees of freedom.

Table 4. 2 RAO Reduction of Geometry Model to Purefloat Model

No	RAO	Cylindrical	Rectangular	Breakwater
1	Surge (m)	64%	83%	38%
2	Sway m)	71%	29%	48%
3	Heave (m)	43%	29%	57%
4	Roll (″)	36%	84%	80%
5	Pitch (″)	21%	41%	41%
6	Yaw (″)	39%	13%	92%
Transitional Average (m)		59%	47%	48%
Rotational Average (″)		32%	46%	71%

After conducting an analysis, for translational motion, the most significant reduction in RAO occurs in the cylindrical model i.e. 59%. In the case of the rotational motion, the most significant reduction in RAO occurs in the Breakwater model, i.e. 71%. The cylindrical model best reduced the RAO for the sway motion (71%). For the rectangular and breakwater models, the largest RAO reductions occurred for the roll motion (84%) and Yaw motion (92%). The Breakwater model demonstrated the best result in terms of reducing the RAO for six degrees of freedom, with RAO reduction for translational motion being 48% and rotational motion being 71%. The calculation of the RAO reduction value for six Degrees of Freedom is the average accumulated RAO value for translational and rotational movements.

3.4 Effect of Mooring Line Variation on the Response Amplitude Operator (RAO)

In the marine FPV model, two mooring line variations are used, i.e. 4 and 6 pcs, with the type being Non-Linier Catenary. The selection for this particular type of mooring line is adjusted to the system's environmental conditions in which it will be placed on the seawater, thus necessitating a type of mooring line that can withstand the wave's drag force and adapt to water conditions when the depth changes [6], [14]. The following gives the RAO reduction percentages for each degree of freedom by adding the number of mooring lines.

Table 4.3 RAO Reduction After Additional of Mooring Line

No	RAO	Purefloate	Cylindrical	Rectangular	Breakwater
1	Surge (m)	47%	38%	37%	2%
2	Sway m)	50%	55%	4%	82%
3	Heave (m)	15%	16%	3%	15%
4	Roll (″)	36%	6%	5%	7%
5	Pitch (″)	17%	2%	2%	27%
6	Yaw (″)	47%	62%	3%	76%
Transitional Average (m)		37%	36%	14%	32%
Rotational Average (″)		33%	23%	3%	36%

Based on these results, the addition of mooring lines may impede the system's motion and limit its amplitude for marine FPVs. The simulation results demonstrate that the Purefloat model exhibits the most significant average RAO reduction for translational motion and rotational motion is the Purefloat model (37%). As for both motions, the most significant

reduction in RAO occurred in the Breakwater model (35.3%). In addition to the RAO reduction, the addition of mooring lines can also reduce the lines' tension load by dividing the tension into more mooring lines, thus extending the mooring line usage lifetime and the load for each mooring line. In the mooring line tension aspect, the average total tension reduction observed for the four models after the addition of two mooring lines was 9%, with the most significant reduction being observed for the pontoon Breakwater geometry model (13%) and the least significant being observed for the rectangular model (5%).

The difference in the line's tension on mooring lines will affect the value of the system's response to the excitation force exerted by the waves. Mathematically, the RAO for ω frequency and θ angle is modeled by Eq. (2.9) [22]. This equation explains that the RAO is linearly proportional to the force exerted on a floating structure. In hydrodynamics, forces exerted on a floating structure can be described in the Morrison equation which is the summation from Froude-Krylov, the hydrodynamic mass force, and the drag force [13]. In a similar context, the mooring line tension can be affected by one of many hydrostatic forces, such as the Morrison effect. A high-tension value on a mooring line affects the RAO, albeit with insignificant relations. This means that tension does not directly cause the RAO to increase or decrease. Thus, in the RAO calculation, it is necessary to consider multiple variables and other parameters. This is shown in Eq. (2.1), where the mathematical equation used to describe the relations between the mooring line tension and hydrodynamic forces are addition and subtraction; therefore, the calculated parameter value depends considerably on other parameters and is neither linearly proportional nor inversely proportional.

3.5 Effects of Varying Depths and Waves towards RAO

In the conducted research, various water depths and waves are given. For varying waves, the wave type used is irregular waves. In the simulation, varying water depths and waves were given to each geometry model to find the RAO value. The propensity of RAO's results showcases that at a depth of 20 meters, the resulting RAO surge value from the four models is increasing. This is because in deep water, waves do not have an intensive interaction toward the bottom of the water hence the energy that the waves possess will not be reduced to the bottom of the water. Table 4.4 shows the additional percentage of the RAO value for each geometry model for 15 and 20-m water depth variations by comparing it to the depth of 10 meters.

Table 4.4. RAO Increasing Based on Depth Variation

		Purefloate		Cylindrical		Rectangular		Breakwater	
No	**RAO**	*15*	20	15	20	15	20	15	20
1	Surge (m)	9%	8%	62%	51%	65%	73%	13%	13%
2	Sway m)	85%	50%	85%	11%	28%	25%	80%	3%
3	Heave (m)	26%	23%	18%	24%	10%	5%	11%	9%
4	Roll (″)	44%	61%	68%	1%	6%	1%	1%	50%
5	Pitch (″)	14%	16%	14%	18%	3%	10%	25%	24%
6	Yaw (″)	43%	38%	88%	49%	27%	15%	75%	6%
Transitional Average (m)		40%	27%	55%	29%	34%	34%	35%	8%
Rotational Average (″)		34%	38%	53%	23%	12%	9%	34%	27%

The results of this analysis demonstrate a significant increase in the RAO value for translational and rotational motions. The use of a depth variation of 15 m on average increases the RAO by 38% increase in RAO. In the case of 20 meters variation, the percentage of RAO's increase is 24%. Table 4.5 shows the result of RAO's increase comparison relative to waves' variation.

Table 4.5 RAO Increasing Based on Irregular Wave Variation

		Purefloate		Cylindrical		Rectangular		Breakwater	
No	**RAO**	**Irr Wave 2**	**Irr Wave 3**	**Irr Wave 2**	**Irr Wave 3**	**Irr Wave 2**	**Irr Wave 3**	**Irr Wave 2**	**Irr Wave 3**
1	Surge (m)	54%	58%	57%	55%	38%	84%	35%	54%
2	Sway m)	83%	85%	91%	79%	6%	18%	57%	36%
3	Heave (m)	22%	5%	8%	36%	1%	0%	31%	25%
4	Roll (″)	32%	57%	64%	50%	8%	23%	5%	41%
5	Pitch (″)	40%	39%	22%	46%	14%	29%	23%	15%
6	Yaw (″)	82%	88%	96%	85%	3%	17%	8%	67%
Transitional Average (m)		52%	49%	53%	57%	15%	34%	41%	38%
Rotational Average (″)		51%	60%	61%	61%	8%	24%	12%	41%

The result of the calculation shows that for irregular wave type 2, the most significant translational and rotational RAO occurs on the cylindrical model i.e., 53% and 61%. For irregular wave type 3 (Hs = 0.6 m), the most significant increase by using RAO for translational and rotational waves occurs in the cylindrical model. This shows that the cylindrical model exhibits the worst performance when dealing with disturbances. This is further reinforced by the previous analyses, in which the cylindrical model exhibited the smallest RAO reduction compared to the other two models. The use of Irregular Wave type 2 (Hs = 0.5 m) increased the RAO value by as much as 37% in the four models. Meanwhile, the use of Irregular Wave 3 (Hs = 0.6 m) adds up to 46%.

3.6 Results Comparison between RAO and PIANC Standard

The RAO results obtained from the simulation require further analysis of whether or not the models that have been made meet the proper RAO standard. Nevertheless, the RAO's standard for FPV notably for Marine FPV has yet to be determined in detail and is still in the form of *Best Practice for Floating Photovoltaics,* as provided by DNV [30] and the World Bank [6]. The only usable standard for the measurable parameter of the RAO value of PF solar cells is the PIANC Standard, as used by Tajali (2011). The PIANC Standard is also a reference used in *Best Practice for Floating Photovoltaics* by DNV [30]. The RAO's values on the PIANC Standard are *Surge* 0.5 m, *Sway* 0.6 m, *Heave* 0.4 m, *Roll* 1.5º, *Pitch* 0.5º, and *Yaw* 1

Based on the calculations, some RAO values did not meet the PIANC standards. For Heave translational motion, four models exhibit RAO values that exceed the maximum threshold for Heave. However, in the case of the surge and sway motions, these four models comply with the PIANC standards across all variations, whether for 4 or 6 mooring line configuration.

Regarding the pitch rotational motion, these geometric models failed to meet the RAO Pitch standard in both the 4 and 6 mooring line configurations. Conversely, for Roll and Yaw motions, the RAO values for the four geometries do meet the established standards.

The failure of Heave and Pitch to meet the standards is attributed to the selection of a seawater environment with extreme wave parameters. When the Wave's Significant Height (Hs) ranges from 0.3 m to 0.6 m, high RAO values were generated. The heave and pitch motions are vertical resonant motions that relate to the structure's height in position and occur perpendicular to the wave direction. [31]. Consequently, when high-amplitude impulses are given with significant frequency variations, the marine FPV system moves along with the big RAO.

3.7 Discussion and Recommendation

This research was intended to discover the effects of design variations and the working environment on the hydrodynamic response. This analysis simulated the pressure *distribution*, *power output*, and RAO to a Marine FPV system. These four models had different pressure distribution types, depending on the type of pontoon geometry. The purefloat and breakwater models exhibited a high-pressure tendency on the pontoon's middle section. In the cylindrical and rectangular models, the pressure distribution occurs on the pontoon's tip side from the incoming wave's side.

For the four geometry variations in use, the output result's analysis shows that the Purefloat model generates the best power production. This is due to the pitch motion of the Purefloat model being the smallest compared to the other three models; therefore, the incident angle variation of the sun against the solar panels is smaller, and the generated output is bigger.

The addition of mooring lines enables a more even load distribution and reduces motion amplitude. The addition of mooring lines can increase the stability and reduce the risk of structural damage due to a high hydrodynamic load. In the conducted research, the addition of mooring lines can reduce the lines' tension by up to 9%, with the RAO reduction percentage ranging between 8%-27%. In addition, regarding the geometry variation, the most significant reduction in the RAO value was obtained from the four geometry models in the range of 46%-59%.

The result of this research shows that the mooring line's geometry variations, depth variations, and wave of the mooring line significantly affect the hydrodynamic response. The use of a large wave load on a deep-sea water application may result in a big RAO value for those four geometry models. Reducing the impact of the said load requires an additional secondary pontoon and mooring line to reduce the excitation force exerted on a Marine FPV system. Although the analysis conducted on 6 DOFs is separately elaborated, however, the motions of Marine FPV's system in an actual condition happen simultaneously. The variations in use during this research can be made as preliminary design parameters for a marine FPV by adjusting the system capacity, panel layout, and floating system orientation against incoming waves. The adjustments made surely take into consideration the relationship between variations that are used during the research. The said relationship is broken down through (2.8), (2.9), and (2.10) equations, where the varied variables are interconnected and intertwined with one another. By using this mathematical equation, the design parameters of a marine FPV can be further explained more comprehensively for certain seawater conditions.

This final assignment is expected to successfully provide an understanding of the design parameters and Marine FPV's environment. This research is still limited in many aspects; therefore, it is expected that in the next research, further development and analyses will be conducted in a more in-depth fashion. A couple of matters that are worth paying attention to in the next research are , for example, the selection of the pontoon's dimension, the pontoon's orientation, the

panel's orientation, the water limit (dipped depth), and the type of material. Regarding the environmental aspects, some aspects that can further be considered are for example the use of Cross-Swell simulation (cross waves), seabed variation, type of mooring, incoming wave direction, and wind and flow direction.

4.0 CONCLUSION

This study demonstrates that pontoon geometry significantly affects marine FPV hydrodynamic performance. The breakwater configuration showed superior motion reduction with 59% average RAO decrease across six DOF, followed by rectangular (56%) and cylindrical (47%) models. Increasing mooring lines to six reduced RAO values by 27% on average and line tension by 9%. These findings provide hydrodynamic performance insights for preliminary design considerations, while acknowledging that comprehensive design requires additional cost, manufacturing, and structural assessments beyond this study's scope.

References

[1] A. S. Pramudiyanto and S. W. A. Suedy, "Energi Bersih dan Ramah Lingkungan dari Biomassa untuk Mengurangi Efek Gas Rumah Kaca dan Perubahan Iklim yang Ekstrim," *J. Energi Baru dan Terbarukan*, vol. 1, no. 3, pp. 86–99, 2020, doi: 10.14710/jebt.2020.9990.

[2] G. Dan, P. Pelayanan, F. Publik, and D. I. Indonesia, "G20 dan penguatan pelayanan fasilitas publik di indonesia," vol. 1, no. 5, 2022.

[3] PLN, "Rencana Usaha Penyediaan Tenaga Listrik (RUPTL) PT PLN (Persero) 2021-2030.," *Rencana Usaha Penyediaan Tenaga List. 2021-2030*, pp. 2019–2028. 2021.

[4] ESDM, "Kementerian ESDM Akan Tuntaskan 100% Rasio Elektrifikasi di 2022," 2022. https://www.esdm.go.id/id/media-center/arsip-berita/kementerian-esdm-akan-tuntaskan-100-rasio-elektrifikasi-di-2022-

[5] CNBC, "4.700 Desa Belum Teraliri Listrik, Begini Jurus PLN!," 2022. https://www.cnbcindonesia.com/news/20220615172612-4-347429/4700-desa-belum-teraliri-listrik-begini-jurus-pln

[6] "Where Sun Meets Water," *Where Sun Meets Water*, 2019, doi: 10.1596/32804.

[7] Z. Tajali and M. Shafieefar, "Hydrodynamic analysis of multi-body *floating* piers under *Wave* action," *Ocean Eng.*, vol. 38, no. 17–18, pp. 1925–1933, 2011, doi: 10.1016/j.oceaneng.2011.09.025.

[8] S. M. Kim, M. Oh, and H. D. Park, "Analysis and prioritization of the *Floating Photovoltaic* system potential for reservoirs in Korea," *Appl. Sci.*, vol. 9, no. 3, 2019, doi: 10.3390/app9030395.

[9] D. N. V As, "Edition March 2021 Amended October 2021 Design, development and operation of *floating* solar photovoltaic systems (Preview copy)," no. March, 2021.

[10] Z. A. D. Kuswanto, "Pengaruh Bentuk Benda Dan Kedalaman Terhadap Gaya Angkat Ke Atas (Fa) Pada Fluida Statis," pp. 4–20, 2013, [Online]. Available: https://repository.unej.ac.id/bitstream/handle/123456789/13204/Zaenal Abidin Dwi Kuswanto - 080210192060_1.pdf?sequence=1&isAllowed=y

[11] M. Acharya and S. Devraj, "*Floating* Solar Photovoltaic (FSPV): A Third Pillar to Solar PV Sector ?," *TERI Discuss. Pap. ETC India Proj. (New Delhi Energy Resour. Institute)*, p. 68, 2019, [Online]. Available: www.teriin.org

[12] N. A. S. Elminshawy, A. Osama, D. G. El-Damhogi, E. Oterkus, and A. M. I. Mohamed, "Simulation and experimental performance analysis of partially *floating* PV system in windy conditions," *Sol. Energy*, vol. 230, no. August, pp. 1106–1121, 2021, doi: 10.1016/j.solener.2021.11.020.

[13] D. Friel, M. Karimirad, T. Whittaker, and J. Doran, "Hydrodynamic investigation of design parameters for a *Cylindrical* type *floating* solar system," *Dev. Renew. Energies Offshore - Proc. 4th Int. Conf. Renew. Energies Offshore, RENEW 2020*, no. October, pp. 763–770, 2021, doi: 10.1201/9781003134572-87.

[14] R. Y. Yang and S. H. Yu, "A study on a *floating* solar energy system applied in an intertidal zone," *Energies*, vol. 14, no. 22, 2021, doi: 10.3390/en14227789.

[15] P. D. I. Torino, "Master of Science in Energy and Nuclear Engineering Master of Science Thesis *Floating Photovoltaic* systems : state of art , feasibility study in Florida and computational fluid dynamic," 2020.

[16] S. K. Das and M. Baghfalaki, "Mathematical modeling of response amplitude operator for *Roll* motion of a *floating* body: Analysis in the frequency domain with numerical validation," *J. Mar. Sci. Appl.*, vol. 13, no. 2, pp. 143–157, 2014, doi: 10.1007/s11804-014-1249-7.

[17] S. Gorjian, H. Sharon, H. Ebadi, K. Kant, F. Bontempo, and G. Marco, "Recent technical advancements, economics and environmental impacts of floating photovoltaic solar energy conversion systems," *J. Clean. Prod.*, vol. 278, p. 124285, 2021, doi: 10.1016/j.jclepro.2020.124285.

[18] S. Gorjian, H. Sharon, H. Ebadi, K. Kant, F. B. Scavo, and G. M. Tina, "Recent technical advancements, economics and environmental impacts of *Floating Photovoltaic* solar energy conversion systems," *J. Clean. Prod.*, vol. 278, p. 124285, 2021, doi: 10.1016/j.jclepro.2020.124285.

[19] J. Friel, D. Karimirad, M. Whittaker, T. Doran, "Hydrodynamic investigation of design parameters for a *Cylindrical* type *floating* solar system," *Dev. Renew. Energies Offshore - Proc. 4th Int. Conf. Renew. Energies Offshore, RENEW 2020*, no. October, pp. 763–770, 2021, doi: 10.1201/9781003134572-87.

[20] MIT OCW, "Morrison Equation, Spring 2004," 2004.

[21] E. Malayjerdi and M. R. Tabeshpour, "Response Amplitude Operators of Displacement, Velocity, and Acceleration of TLP," no. December, pp. 22–25, 2015.

[22] M. Baghfalaki, S. K. Das, and S. N. Das, "Analytical model to determine response amplitude operator of a *floating* body for coupled *Roll* and *Yaw* motions and frequency-based analysis," *Int. J. Appl. Mech.*, vol. 4, no. 4, 2012, doi:

10.1142/S1758825112500445.
[23] A. A. Babatunde, S. Abbasoglu, and M. Senol, "Analysis of the impact of dust, tilt angle and orientation on performance of PV Plants," *Renew. Sustain. Energy Rev.*, vol. 90, no. October 2017, pp. 1017–1026, 2018, doi: 10.1016/j.rser.2018.03.102.
[24] A. I. Manolache, G. Andrei, and L. Rusu, "An Evaluation of the Efficiency of the *Floating* Solar Panels in the Western Black Sea and the Razim-Sinoe Lagunar System," *J. Mar. Sci. Eng.*, vol. 11, no. 1, 2023, doi: 10.3390/jmse11010203.
[25] I. Ansys, "AQWA User Manual," *Ansys Inc.*, vol. 15317, no. October, pp. 724–746, 2012.
[26] J. R. Shewchuk, "Triangle : Engineering a 2D Quality Mesh Generator and Delaunay Triangulator".
[27] D. N. Moriasi, J. G. Arnold, M. W. Van Liew, R. L. Bingner, R. D. Harmel, and T. L. Veith, "M e g s q a w s," vol. 50, no. 3, pp. 885–900, 2007.
[28] M. A. Lukiantchuki, A. P. Shimomura, F. M. da Silva, and R. M. Caram, "Evaluation of simulations with wind tunnel experiments: Pressure coefficients at openings in the sawtooth building," *Acta Sci. - Technol.*, vol. 40, 2018, doi: 10.4025/actascitechnol.v40i1.37537.
[29] T. L. Scofield, "Math 143-ANOVA," vol. 2, pp. 1–11, 2018, [Online]. Available: https://www.calvin.edu/~scofield/courses/m143/materials/handouts/anova1And2.pdf
[30] DNV, "Design, development and operation of *floating* solar photovoltaic systems (Edition March 2021 Amended October 2021)," no. March, 2021.
[31] K. Xu, Z. Gao, and T. Moan, "Effect of hydrodynamic load modeling on the response of *floating* wind turbines and its mooring system in small water depths," *J. Phys. Conf. Ser.*, vol. 1104, no. 1, 2018, doi: 10.1088/1742-6596/1104/1/012006.
[32] KESDM, "Panduan Perencanaan Pembangkit Listrik Tenaga Surya PLTS Terapung," 2021.
[33] Y. Wang, et al., "Hydrodynamic performance analysis of floating photovoltaic systems under wave-current interactions," *Ocean Engineering*,Vol. 302, p.117632, 2024
[34] K. Lee, at al., "Advanced mooring design for floating solar farms in coastal environment," *Renewable Energy*, vol. 225, pp. 120245-120256, 2024.